Thermal conductivity of graphene and graphite

A. Alofi* and G. P. Srivastava
School of Physics, University of Exeter, Stocker Road, Exeter EX4 4QL, United Kingdom
(Received 18 January 2013; published 18 March 2013)

The thermal conductivities of graphene and graphite are computed within the framework of Callaway's effective relaxation time theory. Analytical expressions derived by Nihira and Iwata for phonon dispersion relations and vibrational density of states are employed, based on the semicontinuum model proposed by Komatsu and Nagamiya. The conductivity of graphene is predicted to be higher than the in-plane conductivity of graphite for all temperatures. Incorporation of the ^{13}C isotope can be expected to produce significant reduction in the conductivity of graphene in the temperature range 50–300 K. In the presence of tensile strain on graphene, the specific heat increases, but the conductivity can decrease or increase depending on the level of the purity and temperature of the sample.

DOI: 10.1103/PhysRevB.87.115421 PACS number(s): 65.80.Ck, 63.22.Rc, 63.20.D−

I. INTRODUCTION

Along with its unique electronic properties and high electrical conductivity,[1,2] graphene shows unusually high thermal conductivity. Reported values for the thermal conductivity of graphene at room temperature are in the range 2000–6000 W/m K,[3–5] being higher than the results measured for graphite[6] and diamond.[7] Fundamentals and applications of the thermal properties of graphene have recently been reviewed.[8] The high thermal conductivity of monolayer and multilayer graphene must prove useful for establishing improved reliability and speed of electronic and optoelectronic devices. Multilayer graphene and graphite may be described as layered materials, exhibiting highly anisotropic structural and elastic properties. Such materials are characterized by rather rigid layers, loosely packed together perpendicular to each other. Atomic layers in graphite, the most typical representative of layered crystals, consist of two-dimensional sequences of regular hexagons (graphene). The intralayer distance in the planes is much shorter than the interlayer distance: the atoms inside a layer are at a distance of 1.4 Å and the distance between the layers is 3.35 Å. This feature is typical of all layered materials and causes the anisotropy of the bonding forces in such crystals.[9–12] The elastic properties of a hexagonal crystal in the layer or symmetry plane are isotropic and are described by the elastic moduli C_{11} and C_{12}. The constant C_{33} describes the interlayer interaction and determines Young's modulus in the normal direction, and C_{44} describes stresses caused by displacements of the layers with respect to each other.[9,13,14]

The anisotropy of bonding forces in layered materials results in specific features of phonon spectra, such as the existence of low-frequency modes in which the layers move relative to each other, low velocities of the acoustic modes propagating in the direction of weak bonding, and a quadradic dispersion behavior of the vibrations propagating in the layer plane with a displacement vector perpendicular to the layers (the so-called $TA_\perp$ or ZA mode). In other words, the phonon dispersion relations of layered crystals are characterized by low interlayer modes and high-frequency intralayer modes. These features are manifested in the physical properties controlled by the phonon subsystem, such as heat capacity, thermal expansion, and thermal conductivity.[15–17] The graphite crystal possesses hexagonal symmetry and there are two principal thermal conductivities to be evaluated. The conductivity measured in any direction parallel to the basal planes is denoted by K_a and that parallel to the hexagonal axis is K_c, thus the components of the conductivity tensor are $K_{xx} = K_{yy} = K_a$, and $K_{zz} = K_c$. The anisotropy of the physical properties of graphite, including thermal conductivity, provides an example of extreme deviation from those of isotropic solids.[18,19] The thermal conductivity along the c axis in graphite is found to be two orders of magnitude smaller than graphene thermal conductivity, making it promising for devices with improved thermoelectric figure of merit.

Generally, the lattice thermal conductivity of a solid increases with temperature, goes through a maximum value, and then starts to decrease. The temperature at which the conductivity maximum occurs is material dependent, but usually lies in the range 10–150 K. At temperatures near and above the maximum, the role of anharmonic phonon interaction becomes progressively important in determining the conductivity. The simplest picture of anharmonic interaction can be presented in terms of three-phonon scattering events. A three-phonon scattering process is called a normal (N) process if can take place with all three phonons lying within the first Brillouin zone of the corresponding lattice. Such a process is momentum-conserving in nature. Momentum-nonconserving events are referred to as umklapp (U) processes. The Debye model of thermal conductivity does consider both N and U processes, but resorts to the so-called *single-mode relaxation time* picture and ignores the momentum-conserving property of N processes when accounting for the total relaxation rate (or the related lifetime) of phonons. Callaway[20] pointed out that the momentum-conserving nature of N processes is an essential part of the lattice thermal conduction process and its contribution should be added to determine an effective relaxation time of phonons. The resulting conductivity expression includes an extra term over and above the Debye term, and is known as the N-drift term.[20,21] It has been shown[22] that the N-drift contribution can be quite large for pure crystals.

In this paper we apply Callaway's theory in its full form[20] to study the thermal conductivity in graphene and graphite. Our calculations employ the analytical expressions for the phonon dispersion relations and the vibrational density of states based

on the work by Nihira and Iwata[23] within the semicontinuum model developed by Komatsu and Nagamiya.[24] We also investigate the effects of isotopes and tensile strain on the thermal conductivity of graphene.

II. THEORY

The theory of the thermal vibrations of the carbon atoms in the graphite crystal has been addressed by a number of authors.[6,18,19,25,26] The hexagonal symmetry of graphite requires that the thermal conductivity is independent of direction parallel to the basal plane, i.e., the principal conductivities K_{xx} and K_{yy} in the plane are equal, while the third principal conductivity K_{zz} is different.[19] Assuming that only the phonon contribution needs to be considered, the calculations for thermal conductivity are all carried out using a semicontinuum model in which the $K^{\rm th}_{\alpha\beta}$ component of the thermal conductivity tensor is given by[19,21]

$$K_{\alpha\beta} = \sum_{\boldsymbol{q},p} \left[\frac{\hbar\omega_p(\boldsymbol{q})}{k_B T}\right]^2 \tau_p(\boldsymbol{q}) \frac{\exp[\hbar\omega_p(\boldsymbol{q})/k_B T]}{\{\exp[\hbar\omega_p(\boldsymbol{q})/k_B T]-1\}^2} \times \{v_p(\boldsymbol{q})\}_\alpha \{v_p(\boldsymbol{q})\}_\beta. \quad (1)$$

Here, $\tau_p(\boldsymbol{q})$ is the relaxation time of a phonon of wave vector $\boldsymbol{q}$ in the pth vibrational branch, $\omega_p(\boldsymbol{q})$ is the frequency of the phonon, $\{v_p(\boldsymbol{q})\}_\alpha, v_p\{(\boldsymbol{q})\}_\beta$ are the components of the phonon velocity; in direction α, $\beta(\alpha,\beta = x,y$ or $z)$, T is the absolute temperature, k_B is Boltzmann constant, and $\hbar$ is the reduced Planck's constant. The summation over wave vectors $\boldsymbol{q}$ and each vibrational branch in Eq. (1) should be carried out over the appropriate Brillouin zone. For the semicontinuum model employed in the present work, the graphite Brillouin zone is replaced by a circular cylinder with height $q_z^{\max} = \pi/c$. For graphene, the Brillouin zone in the q_x-q_y plane could be replaced by a circle of equivalent area with Debye radius q_a determined from the relation $\pi^2 q_a = 2\pi^2/A$, where $A = a^2\sqrt{3}/2$, is the area of the Brillouin zone of graphene, and $q_a = (q_x^2 + q_y^2)^{1/2}$ varies over the range $0 - q_a^{\max} = 4(\pi/3\sqrt{3})^{1/2}/a_{cc}$, where a_{cc} is the nearest-neighbor atomic spacing. In every case the summation will be replaced by an integration and q expressed as a function of frequency ω_p from the phonon dispersion relations. Within Callaway's formalism,[20,21] we express the lattice thermal conductivity tensor as

$$\{K_{\alpha\beta}\}_{\rm C} = \{K_{\alpha\beta}\}_{\rm D} + \{K_{\alpha\beta}\}_{\rm N-drift}. \quad (2)$$

Here $\{K_{\alpha\beta}\}_{\rm D}$ is the Debye thermal conductivity expression given by

$$\{K_{\alpha\beta}\}_{\rm D} = \frac{\hbar^2}{2A_m k_B T^2} \sum_p \int d\omega \omega_p^2 \{v_p(\omega)\}_\alpha \{v_p(\omega)\}_\beta \times \tau_p(\omega)\bar{n}(\bar{n}+1)D(\omega_p), \quad (3)$$

where A_m is the molar area, $\bar{n}$ is the Bose-Einstein distribution function, and $D(\omega_p)$ is the density of states function per mole for all branches. $\{K_{\alpha\beta}\}_{\rm N-drift}$ is the normal-drift contribution given by

$$\{K_{\alpha\beta}\}_{\rm N-drift} = \frac{\hbar^2}{2A_m k_B T} \sum_p \frac{\left[\int d\omega D(\omega_p)\omega_p^2 \{v_p(\omega)\}_\alpha \{v_p(\omega)\}_\beta \tau_p \tau_N^{-1} \bar{n}(\bar{n}+1)\right]^2}{\int d\omega D(\omega_p)\omega_p^2 \{v_p(\omega)\}_\alpha \{v_p(\omega)\}_\beta \tau_N^{-1}\left(1-\tau_p\tau_N^{-1}\right)\bar{n}(\bar{n}+1)}. \quad (4)$$

In the above expressions $\tau \equiv \tau_p(\boldsymbol{q})$ is the so-called *single-mode relaxation time* for a phonon of wave vector $\boldsymbol{q}$, polarization branch p, and the factor $1/2$ in both Eqs. (3) and (4) reflects the nature of the two-dimensional geometry of graphene. For pristine undoped and suspended graphene, the phonon relaxation rate is contributed from the scattering of phonons from a finite size of sample, point defects, and anharmonicity: $\tau^{-1} = \tau_{\rm bs}^{-1} + \tau_{\rm pd}^{-1} + \tau_{\rm anh}^{-1}$. The dominant anharmonic contribution is considered from three-phonon scattering processes of normal and umklapp types: $\tau_{\rm anh}^{-1} = \tau_N^{-1} + \tau_U^{-1}$.[21] The normal-drift contribution $\{K_{\alpha\beta}\}_{\rm N-drift}$ arises from the momentum conservation requirement for three-phonon normal scattering processes. Numerical computation of the thermal conductivity tensor thus requires a knowledge of the quantities $\omega_p(\boldsymbol{q})$, $\tau_p(\boldsymbol{q})$, $v_p\{(\boldsymbol{q})\}_x$, and $v_p\{(\boldsymbol{q})\}_z$ for the system. All these important quantities are discussed below.

A. Phonon dispersion relations, density of states, and velocities

1. Dispersion relations

Komatsu and Nagamiya[24] modelled graphite as a semicontinuum: graphite replaced by a parallel stack of thin elastic plates at an interplanar distance c. Each elastic plate possesses a resistance to bending, stretching, and shearing, while adjacent plates are coupled by elastic forces resisting shear and compressive tensile displacements. Nihira and Iwata[23] adopted the Komatsu-Nagamiya semicontinuum model and derived analytic expressions for the phonon dispersion relations and the vibrational density of states for graphite. The vibrational frequencies for the three acoustic modes are expressed as

$$\omega_1^2 = v_l^2\left(q_x^2+q_y^2\right) + \frac{4\zeta}{c^2}\sin^2(cq_z/2),$$
$$\omega_2^2 = v_t^2\left(q_x^2+q_y^2\right) + \frac{4\zeta}{c^2}\sin^2(cq_z/2), \quad (5)$$
$$\omega_3^2 = b^2\left(q_x^2+q_y^2\right)^2 + 4\mu^2\sin^2(cq_z/2).$$

The subscripts 1 and 2 refer to vibrations polarized in the basal planes, the former to in-plane longitudinal mode LA and the latter to in-plane transverse mode TA, the subscript 3 refers to vibrations of atoms perpendicular to the layer planes (out-of-plane or flextural mode ZA). In these equations, v_l and v_t are the wave velocities, c is the interlayer spacing in graphite, b is the bending elastic parameter which is a measure of the

TABLE I. Physical constants of graphite as presented in the work of Nihira and Iwata (Ref. 23).

C_{11}	106×10^{11}	dyn/cm^2
C_{12}	18×10^{11}	dyn/cm^2
C_{13}	1.5×10^{11}	dyn/cm^2
C_{33}	3.65×10^{11}	dyn/cm^2
C_{44}	0.425×10^{11}	dyn/cm^2
K	3.13×10^{-3}	cm^2/s
c	3.3544×10^{-8}	cm
ρ	2.26	g/cm^3
V	5.30	cm^3/mol
υ_l	2.16×10^6	cm/s
υ_t	1.40×10^6	cm/s
ζ	1.88×10^{10}	cm^2/s^2
μ	1.20×10^{13}	s^{-1}
ω_z	8.18×10^{12}	rad/s
b	3.13×10^{-3}	cm^2/s
ω_z'	2.40×10^{13}	rad/s

resistance of a graphene layer to bending, ζ, μ, υ_l, and υ_t are expressed in terms of the elastic constants C_{ij} as well as the volume density ρ as

$$\zeta = C_{44}/\rho; \quad \mu^2 = C_{33}/c^2\rho; \quad \upsilon_l = [C_{11}/\rho]^{1/2};$$
$$\upsilon_t = \left[\frac{C_{11}-C_{12}}{2\rho}\right]^{1/2}. \tag{6}$$

Table I lists the physical constants of graphite used in this work.

2. Density of states

The corresponding expressions for the density-of-states functions per mole $D(\omega_p)$ for all branches are given by the following analytic expressions:

$$p = \text{LA,TA}, \quad \text{and} \quad \omega \leqslant \omega_z: \quad D(\omega) = \frac{A_m \omega}{\pi^2 \upsilon_p^2} \sin^{-1}\left(\frac{\omega}{\omega_z}\right), \tag{7}$$

$$p = \text{LA,TA} \quad \text{and} \quad \omega \geqslant \omega_z: \quad D(\omega) = \frac{A_m \omega}{2\pi \upsilon_p^2}, \tag{8}$$

$p = \text{ZA}$ and $\omega \leqslant \omega_z'$:

$$D(\omega) = \frac{A_m}{2\pi^2 b}\left(\frac{\omega}{\omega_z'}\right)\int_0^{\sin^{-1}\{[1+(\zeta^2/4b^2\omega^2)]^{-1/2}\}} \times \left[1-\left(\frac{\omega}{\omega_z'}\right)^2\left(1+\frac{\zeta^2}{4b^2\omega^2}\right)\sin^2\phi\right]^{-1/2} d\phi, \tag{9}$$

$p = \text{ZA}$ and $\omega \geqslant \omega_z'$:

$$D(\omega) = \frac{A_m}{2\pi^2 b}\left(1+\frac{\zeta^2}{4b^2\omega^2}\right)^{-1/2}\int_0^{\pi/2}\left[1-\left(\frac{\omega_z'}{\omega}\right)^2 \times \left(1+\frac{\zeta^2}{4b^2\omega^2}\right)^{-1}\sin^2\phi\right]^{-1/2} d\phi, \tag{10}$$

with $\omega_z = 2\zeta^{1/2}/c$ and $\omega_z' = 2\mu$.

3. Velocities

The phonon propagation velocities in crystals are derived from the phonon dispersion relation. In Eq. (1), the velocities $\{v_p(\mathbf{q})\}_{\alpha,\beta}$ are generally assumed to be the group velocities of each vibrational mode given by

$$\{v_p(\mathbf{q})\}_x = \frac{\partial\omega_p(\mathbf{q})}{\partial \mathbf{q_x}}, \quad \{v_p(\mathbf{q})\}_z = \frac{\partial\omega_p(\mathbf{q})}{\partial \mathbf{q_z}}. \tag{11}$$

The phonon group velocities in graphite derived from Eq. (5) are

$$\begin{aligned}
(\upsilon_1)_x &= \frac{\upsilon_l^2 q_x}{\sqrt{\upsilon_l^2 q_a^2 + (4\zeta/c^2)\sin^2(cq_z/2)}},\\
(\upsilon_2)_x &= \frac{\upsilon_t^2 q_x}{\sqrt{\upsilon_t^2 q_a^2 + (4\zeta/c^2)\sin^2(cq_z/2)}},\\
(\upsilon_1)_z &= \frac{\zeta \sin(cq_z)}{c\sqrt{\upsilon_l^2 q_a^2 + (4\zeta/c^2)\sin^2(cq_z/2)}},\\
(\upsilon_2)_z &= \frac{\zeta \sin(cq_z)}{c\sqrt{\upsilon_t^2 q_a^2 + (4\zeta/c^2)\sin^2(cq_z/2)}},\\
(\upsilon_3)_x &= \frac{2b^2 q_a^3 + \zeta q_a}{\sqrt{b^2 q_a^4 + 4\mu^2\sin^2(cq_z/2) + \zeta q_a^2}},\\
(\upsilon_3)_z &= \frac{\mu^2 c \sin(cq_z)}{\sqrt{b^2 q_a^4 + 4\mu^2\sin^2(cq_z/2) + \zeta q_a^2}},
\end{aligned} \tag{12}$$

where $(\upsilon_1)_x$ and $(\upsilon_2)_x$ are the velocity components from LA and TA phonons respectively along the basal plane, $(\upsilon_1)_z$ and $(\upsilon_2)_z$ are the velocity components from LA and TA phonons respectively along the normal to the plane, and $(\upsilon_3)_x$ and $(\upsilon_3)_z$ are the velocity components of the ZA phonons along and normal to the basal plane, respectively.

For graphene we make the approximation that the layer planes are uncoupled: this is ensured by setting $\mu = 0, \zeta = 0$, and $q_z = 0$. Thus for graphene the phonon group velocity components reduce to

$$(\upsilon_1)_x = \upsilon_l, \quad (\upsilon_2)_x = \upsilon_t, \quad (\upsilon_3)_a = 2bq_a = 2\sqrt{b\omega_3}. \tag{13}$$

These also apply for graphite basal plane vibrations parallel to q_a.

For graphite basal plane vibrations parallel to q_z only, it can be assumed that $q_a = 0$, and from Eq. (12)

$$(\upsilon_1)_z = \sqrt{\zeta}\cos(cq_z/2), \quad (\upsilon_2)_z = \sqrt{\zeta}\cos(cq_z/2),$$
$$(\upsilon_3)_z = c\mu\cos(cq_z/2). \tag{14}$$

B. Phonon scatterings and relaxation times

In solids, phonons are scattered by collisions with boundaries, defects, impurities, and other phonons. Different scattering mechanisms may dominate at different temperatures. The major challenge in the calculation of thermal conductivity is determining the relaxation times τ from various types of phonon-scattering processes. The scattering processes are assumed to be independent of one another and following

Matthiessen's rule we express

$$\tau^{-1} = \sum_i \tau_i^{-1}, \tag{15}$$

where τ is the lifetime of a phonon, and τ_i^{-1} is the contribution from the ith scattering process. We consider the following phonon scattering mechanisms, relevant for suspended graphene.

1. Boundary scatterings

At low temperatures, phonons acquire long wavelengths and the boundary scattering process becomes dominant. The phonon relaxation rate $\tau_{\rm bs}^{-1}$ due to boundary scattering is expressed as

$$\tau_{\rm bs}^{-1} = \frac{v_p}{L}, \tag{16}$$

where v_p is the speed of phonons in polarization branch p, and L represents an effective length determined from the geometry of the graphene sample. It is assumed that there are boundaries parallel and perpendicular to the hexagonal axis defining scattering lengths L_c and L_a, respectively. A particular phonon may be scattered by either type of boundary and the relaxation time of a phonon is thus given by

$$\tau_{\rm bs} = \frac{L_a}{\{v_p\}_a}; \quad \tau_{\rm bs} = \frac{L_c}{\{v_p\}_z}. \tag{17}$$

The boundary perpendicular to the hexagonal axis dominates the scattering of phonons for which $L_a/\{v_p\}_a \gg L_c/\{v_p\}_z$ while that parallel to the hexagonal axis dominates the scattering of phonons for which $L_c/\{v_p\}_z \gg L_a/\{v_p\}_a$. Clearly, the boundary scattering rate depends upon the phonon mode involved.

2. Point defect scatterings

As temperature increases and approaches the range where thermal conductivity takes its maximum value, the dominant phonon wavelength decreases and becomes comparable to the size of crystal defects. In this temperature range, impurities, defects, and crystal imperfections strongly control the mean-free path of phonons and thus the thermal conductivity of the material. In the present two-dimensional model, the phonon relaxation time for each polarization p from such scatterings is expressed, following Klemens and Pedraza,[25] as

$$\tau_{\rm pd}^{-1} = \frac{2\pi c_d \omega^3}{\omega_{p,\max}^2}\left(\frac{\Delta M}{M}\right)^2, \tag{18}$$

where c_d is the point defect concentration and $\Delta M/M$ is the fractional atomic mass change. Common point defects in carbon-based materials are vacancies. Using a simple scheme, based on the application of the virial theorem and shared links, Ratsifaritana and Klemens[27] argued that the presence of a vacancy in a three-dimensional crystal would lead to $\Delta M/M = 3$. While isotopic defects are generally accounted for, other types of defects and their concentrations in materials are in general unknown to the level of precision required for a complete account of phonon scattering arising from them. For this reason, it is usual practice to use the product $c_d(\Delta M/M)^2$ as a fitting parameter to account for matching theoretical calculations with experimental measurements of thermal conductivity. We have, therefore, chosen to treat the product $A_d = c_d(\Delta M/M)^2$ for point defects other than isotopes as an adjustable parameter in our work, and rewrite Eq. (18) as

$$\tau_{\rm pd}^{-1} = A_d \frac{2\pi\omega^3}{\omega_{p,\max}^2}. \tag{19}$$

The occurrence of isotopes in natural carbon causes a fluctuation in the mass distribution throughout a crystal. This variation disturbs the periodicity of the lattice and thus produces thermal resistance. Naturally occurring carbon materials are made up of two stable isotopes ^{12}C and ^{13}C with abundancy of ∼99% and ∼1% respectively.[28,29] The phonon relaxation rate due to isotopic scattering can be expressed as

$$\tau_I^{-1} = \frac{2\pi\omega^3}{\omega_{p,\max}^2}\left[f_1\left(\frac{\Delta M_1^2}{\bar{M}}\right) + f_2\left(\frac{\Delta M_2^2}{\bar{M}}\right)\right], \tag{20}$$

where τ_I^{-1} is the isotope scattering relaxation time, M_1 and M_2 are the atomic masses for ^{13}C and ^{12}C, respectively, f_1 and f_2 are the fractions of unit cells having masses M_1 and M_2, respectively, and $\bar{M} = \sum_i f_i M_i$ is the average atomic mass.

3. Three-phonon scatterings

At high temperatures, anharmonic phonon scatterings become dominant. Such processes can also be important at low temperatures, providing a substantial contribution to the thermal resistivity near the conductivity maximum.[30] The simplest, and most significant, of such scatterings involves three phonons. The strength of anharmonic interactions involving more than three phonons is two to three orders of magnitude weaker than that of three-phonon interactions.[31]

Expressions for anharmonic relaxation times of phonons can be derived by applying first-order time-dependent perturbation theory.[21,32] Such an attempt requires knowledge of cubic anharmonic terms in crystal potential, and a careful consideration of allowed combination of phonon modes for normal (N) and umklapp (U) processes subjected to the momentum and energy selection rules. Such a task is usually very demanding, and becomes even so for graphene which is characterized by the nonlinear dispersion behavior of the ZA branch. Due to such difficulties, the relaxation times of three-phonon scatterings have often been parametrized by expressions of the type[33,34]

$$\tau_{\rm anh}^{-1} = B_T \omega^m T^n, \tag{21}$$

where $m + n = 5$ and B_T is constant over a particular range of temperatures. In this work we assume that the normal and umklapp processes have the same frequency dependence and we employ the low-temperature form of anharmonic relaxation rate using a simple parametrized expression:[20,21]

$$\tau_{\rm anh}^{-1} = [B_N + B_U \exp(-\bar{\Theta}/\alpha T)]\omega^2 T^3, \tag{22}$$

where B_N and B_U are parameters for three-phonon normal and umklapp processes, respectively, $\bar{\Theta}$ is the the average Debye temperature for all acoustic branches, and α is a constant. The presence of the exponential factor in the expression for τ_U^{-1} is consistent with the well-founded assumption that umklapp processes get frozen out at much lower temperatures.

Following discussions in previous works (see, e.g., Refs. 26, 35, and 36), we set $\alpha = 3$ as a good choice. We expect the temperature dependence in the relaxation-rate expression in Eq. (22) to be valid in the range $T \leqslant \bar{\Theta} \simeq 1000$ K for graphene. We also remark that the anharmonic relaxation rate in the form $\omega^2 T$ used by Klemens and Pedraza[25] and subsequently by Nika *et al.*[37] is more suitable at higher temperatures (i.e., above $\bar{\Theta}$).

C. Effect of strain on phonon dispersion relations for graphene

The presence of strain, applied intensionally or unintentionally, can affect the thermal properties of graphene. It has been suggested[38,39] that stress/strain effects can be used to tune the thermal conductivity of nanostructures, including graphene. In particular, it has been revealed that the thermal conductivity of graphene and carbon nanotubes decreases monotonically as the tensile stress increases.[38] Stress related change in the thermal conductivity of graphene can largely be related to changes in the phonon dispersion relation, velocity, and density of states.

Strain arises when a crystal is compressed or stretched out of equilibrium. Theoretically, the effect of strain could be studied by using the continuum theory of elasticity. Experimental measurements[40] indicate a linear relationship between applied pressure P up to 300 Kbar and the in-plane lattice constant a for graphite. From the results presented in Ref. 40 we have expressed $a = a_0 + rP$, with $a_0 = 2.462$ Å as the unstrained lattice constant of graphene and $r = 1.625 \times 10^{-4}$ Å/Kbar. The strain ϵ is then defined as $\epsilon = (a - a_0)/a_0$. Within the elastic limit, we consider both positive and negative values of ϵ corresponding to positive and negative values of pressure P. Using the standard theory of free-standing membranes, de Andres *et al.*[41] studied the effect of strain on the dispersion curve for the flextural (ZA) modes in graphene. For an isotropic strain, ϵ, the dispersion relation, becomes

$$\omega_3^2 = b^2 q_a^4 + 2(\lambda + \bar{\mu})\epsilon q_a^2, \tag{23}$$

where λ and $\bar{\mu}$ are the two-dimensional elastic Lamé coefficients for graphene. Following Refs. 41 and 42, we have taken $\lambda = 2$ eV Å^{-2} and $\bar{\mu} = 10$ eV Å^{-2}. Ignoring in-plane tension, the dispersion relation for the ZA branch becomes $\omega_3^2 = b^2(q_x^2 + q_y^2)^2 = b^2 q_a^4$ and this indeed is the first term in Eq. (5).

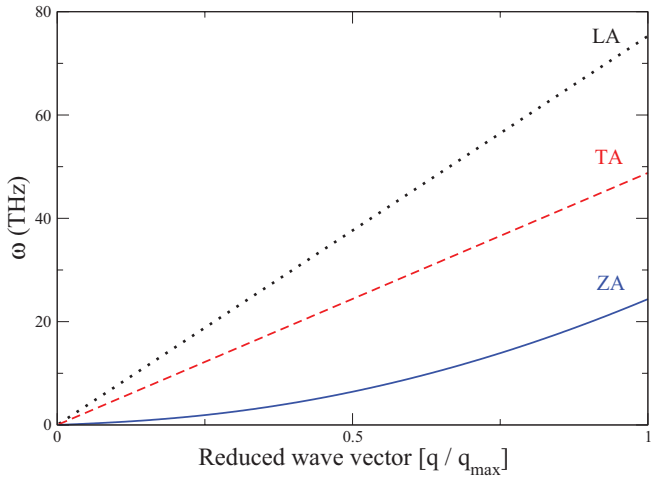

FIG. 1. (Color online) Phonon dispersion curves for graphene.

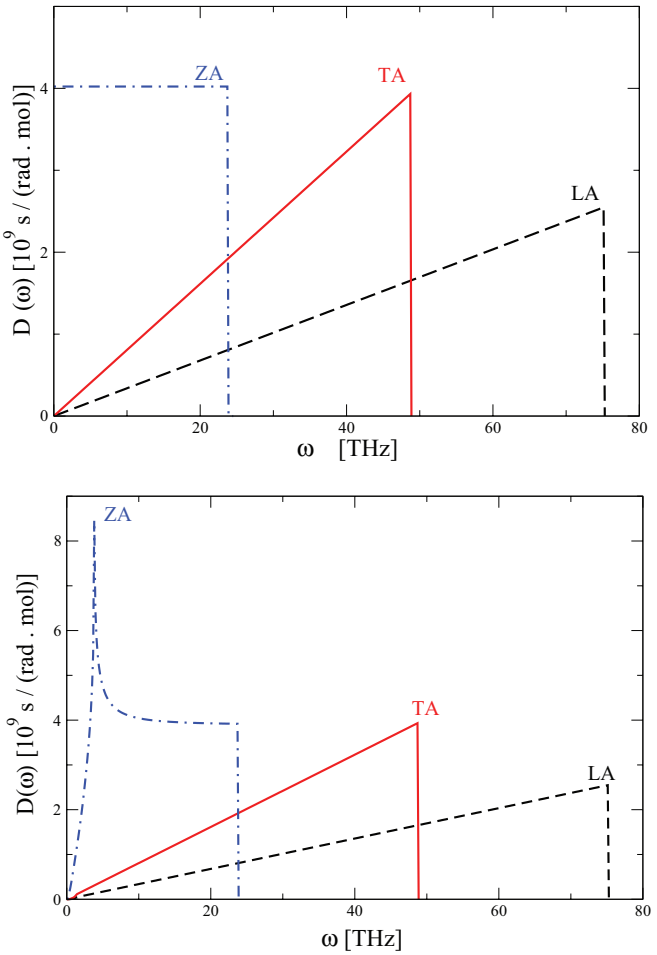

FIG. 2. (Color online) Phonon density of states for separate branches for graphene (upper panel) and graphite (lower panel).

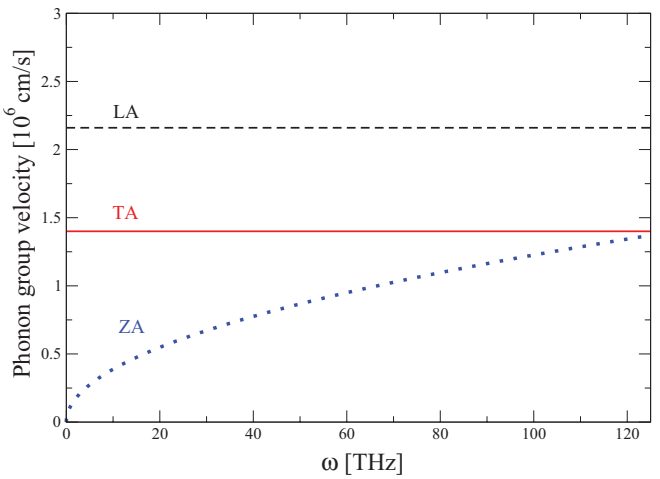

FIG. 3. (Color online) Phonon velocity for separate modes in graphene.

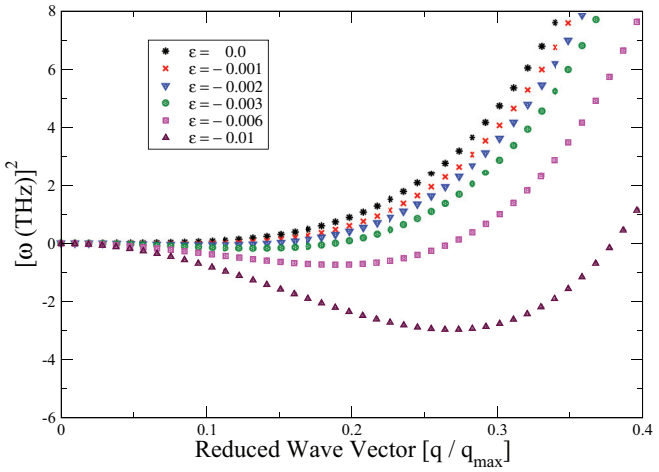

FIG. 4. (Color online) Dispersion relation for out-of-plane phonon modes in graphene under compressive strain.

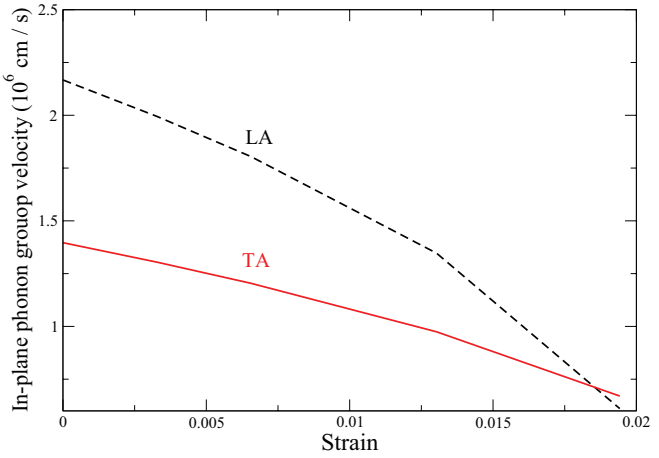

FIG. 6. (Color online) Velocity changes for in-plane phonon modes under strain.

III. RESULTS AND ANALYSIS

A. Phonon dispersion curves, velocity, and density of states

Figure 1 provides the dispersion curves, obtained from Eq. (5), after setting $q_z = 0$. The Debye frequency for each polarization, taken from Ref. 23, are $\omega_{D,LA} = 75.18$ THz, $\omega_{D,TA} = 48.73$ THz, and $\omega_{D,ZA} = 24.28$ THz. The quadratic dispersion of the out-of-plane ZA branch in the long-wavelength region can be clearly noted. This is a characteristic property of the phonon dispersions of layered crystals.[43]

Figure 2 show the phonon density of states for graphene and graphite computed from Eqs. (7)–(10). For graphene, the layer planes are uncoupled, which means $\mu = 0$, $\zeta = 0$, and then setting $q_z = 0$ will reflect the two-dimensional nature of the graphene crystal. For graphite, the above-mentioned parameters would have their nonzero values. It can be noticed clearly that the density of states of ZA phonons is larger than that of LA and TA phonons up to approximately 24 THz and also shows a constant behavior.

Figure 3 shows the phonon velocity variations with frequency for different modes in graphene. The phonon velocity for the LA and TA phonons are constant while the velocity of the ZA phonons shows a nonlinear characteristic, resulting from the nonlinear dispersion relation.

The application of compression is to increase the in-plane frequencies ω(LA) and ω(TA) but decrease the out-of-plane frequency ω(ZA). It was found that with increased compression ω(ZA) becomes imaginary, see Fig. 4, indicating instability of the system. Under tensile strain ω(LA) and ω(TA) decrease but ω(ZA) increases, as seen in Fig. 5. These can be easily understood. Stretching makes the C-C bonds weaker and the in-plane modes softer, and the "dangling bonds" stronger and the out-of-plane mode harder. The change computed for ω(LA) and ω(TA) is larger than that for ω(ZA). The velocities of the LA and TA modes decrease as the strain increases. As can be seen in Fig. 6, we find that the velocity of the LA mode becomes smaller than that of the TA mode for ϵ larger than 0.019. The velocities of the ZA modes of frequencies higher than approximately 2.5 THz also decrease with increase in tension. However, the velocities of this mode for frequencies smaller than 2.5 THz show a reverse trend, and of larger magnitude, as shown in Fig. 7. We note that for $\epsilon = 0.013$ the velocity changes are

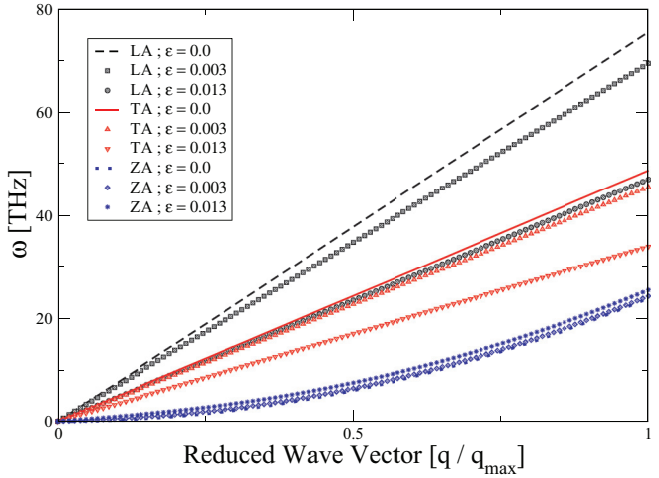

FIG. 5. (Color online) Dispersion relation for in-plane phonon modes in graphene under tensile strain.

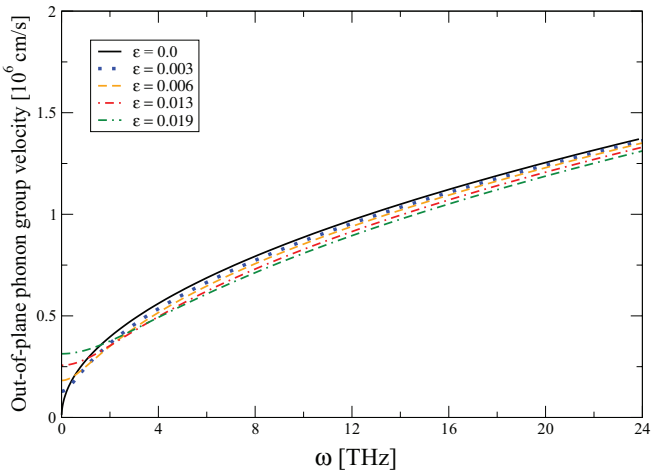

FIG. 7. (Color online) Velocity changes for out-of-plane phonon modes under strain.

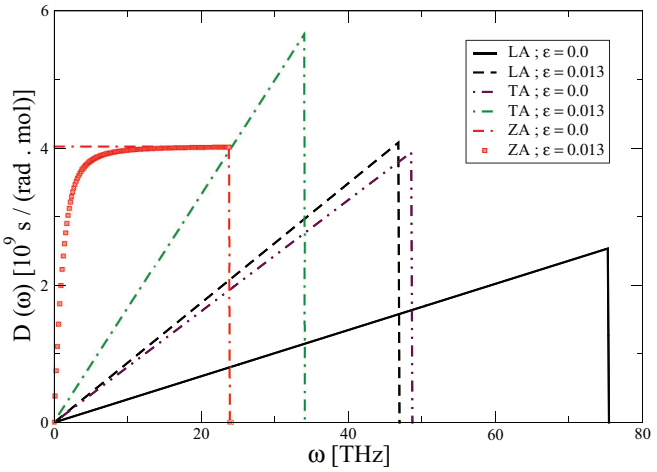

FIG. 8. (Color online) Graphene density of states under tensile strain.

38%, 31%, and 8% for the LA, TA, and high-frequency ZA modes, respectively.

From Fig. 8 we notice that under tensile strain the density of states of the in-plane modes (LA and TA) increases, while it decreases for the out-of-plane modes (ZA). Actually, the density of states for the ZA branch acquires a dispersive behavior at low frequencies: starting from zero for zero frequency, it rapidly reaches the maximum value obtained for the unstrained case above about 15 THz. Below about 5 THz the density of states for the ZA modes is heavily quenched.

B. Specific heat

The specific heat is altered in the presence of tensile stain: whereas the contribution from the LA and TA modes increases, the contribution from the ZA modes decreases. At a given temperature, the combined increase from the LA and TA modes is larger than the decreases from the ZA modes. The overall effect of strain is to increase the specific heat. These features are shown in Fig. 9. The overall increase of C_v with temperature has also been noted in another theoretical study.[44] Our computed results reveal that the effect of strain is largest in the intermediate temperature range (e.g., 16% at 200 K for $\epsilon = 0.013$), becoming very small at both low and high temperatures (e.g., 4% at 100 K and 1% at 2000 K for $\epsilon = 0.013$). These strain-related changes in different temperature ranges arise from the joint effect of related changes in the dispersion relations (ω vs q), density of states [$D(\omega)$], and the phonon distribution function [$\bar{n}(\omega, T)$].

C. Thermal conductivity

Before presenting the results of our calculations, it is worth remarking that in a previous study[45] we concluded that the N-drift term in the Callaway theory, presented in Eq. (4), produces a very important additional contribution to the overall conductivity result for graphene. With this in mind, we will employ the full Callaway formula, Eq. (2), for presenting results in this paper.

1. *Unstrained graphene*

Figure 10 shows the thermal conductivity results for graphene, in graphite basal plane, and along the graphite c axis. The present theoretical results are compared with the experimental measurements reported by Chen *et al.*,[46] who used a sample of a monolayer graphene grown by the chemical vapor deposition (CVD) on copper and then suspended over holes with different diameters ranging 2.9–9.7 μm.

For graphene, the results of phonon conductivity calculations were made for a stand-alone sample of size $L_a = 2.9$ μm and a consideration of $A_d = 4.5 \times 10^{-4}$. In order to fit theory with the experimental data for the suspended sample, we used the following parameters: $B_U = 3.18 \times 10^{-25}$ sK^{-3}, and $B_N = 2.12 \times 10^{-25}$ sK^{-3}. For matching theory with experiment for the basal plane conductivity in graphite,[47] we considered boundary length $L_a = 8.7$ μm and $A_d = 4.5 \times 10^{-4}$, while keeping the parameters B_U and B_N the same as for graphene.

The conductivity along the c axis was computed with the consideration of the boundary length $L_c = 0.1$ μm and $A_d = 4.5 \times 10^{-4}$. Due to the presence of strong intraplanar bonds in graphite basal planes and weak interplanar bonds along the c axis, we had to choose stronger anharmonic interaction parameters ($B_U = 2.23 \times 10^{-22}$ sK^{-3}, and $B_N = 1.48 \times 10^{-22}$ sK^{-3}) in order to match the experimental data

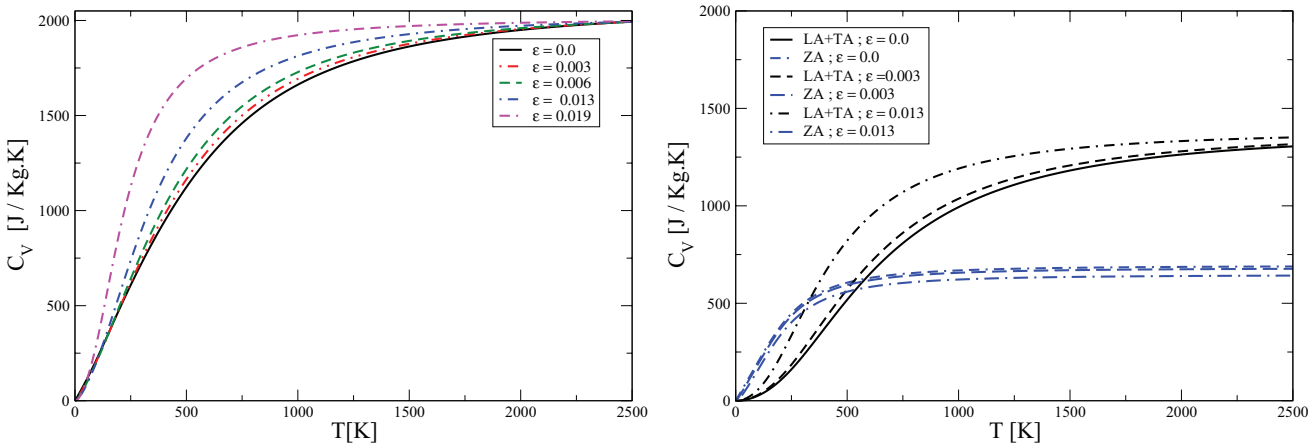

FIG. 9. (Color online) Effect of tensile strain on graphene specific heat for a wide range of temperatures.

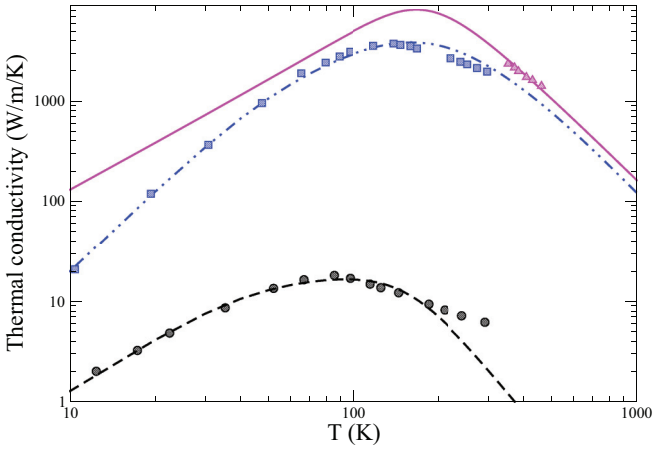

FIG. 10. (Color online) Thermal conductivity of graphene (solid line), graphite basal plane (dotted line) and graphite c axis (dashed line), compared with experimental measurements: graphene (up triangles) (Ref. 46); graphite in-plane (squares) (Ref. 47); graphite c axis (circles) (Ref. 48).

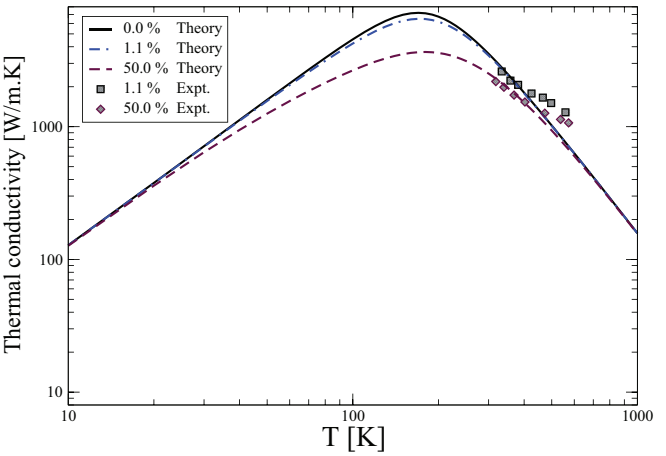

FIG. 11. (Color online) The thermal conductivity of graphene with different concentrations of the ^{13}C isotopes. The symbols represent the experimental measurements from Ref. 28.

for the c-axis thermal conductivity in graphite.[48] Such changes in the choice for the B_U and B_N parameters are supported by the fact that for graphite the in-plane Grüneisen parameter is smaller than that of out-of-plane; see Ref. 49.

The highly anisotropic behavior of the lattice thermal conductivity of graphite is consistent with its anisotropic nature of bonding. At room temperature, the thermal conductivity along the graphite c axis is 2 W/m K, in graphite basal plane is 2195 W/m K, and 3541 W/m K for graphene. The maximum thermal conductivity values computed in the present paper for graphene, graphite basal plane ($K_{xx} = K_{yy} = K_a$), and graphite c axis (K_{zz}) are 7202 W/m K at 170 K, 3808 W/m K at 160 K, and 16 W/m K at 90 K, respectively. It is obvious that, at room temperature, the thermal conductivity of graphite along the c axis is two orders of magnitude smaller than that calculated for graphene. We note that at low temperatures (up to 40 K), the thermal conductivity varies as $T^{1.6}$, $T^{2.4}$, and $T^{1.4}$ for graphene, in the graphite basal plane, and along the graphite c axis, respectively. These clear differences in the temperature variation indicate the quasi-two-dimensional, quasi-three-dimensional, and quasi-one-dimensional nature of the thermal conductivity of graphene, in the graphite basal plane, and along the graphite c axis, respectively.

Apart from the presence of point defects, it is important also to consider the effect of isotopes, present naturally or introduced intentionally, on the thermal conductivity of graphene. A detailed experimental study of the thermal conductivity of isotopically modified graphene containing various percentages of ^{13}C has recently been presented by Chen *et al.*[28] Figure 11 shows the conductivity results for graphene containing two concentrations of the ^{13}C isotopes: 1.1% and 50%. We used 2.9 μm for the effective boundary length. Our theoretical results are in agreement with the experimental measurements made in the temperature range 300–600 K. It is clear from Fig. 11 that the isotopic effect on the conductivity is significant in the low-temperature range 50–300 K. Near the conductivity maximum, around 200 K, the conductivity drops by 15% and 49% for the isotopic concentrations 1.1% and 50%, respectively.

2. *Strained graphene*

It has been reported that the thermal conductivity of graphene is very sensitive to tensile strain.[50,51] Our work shows that the effect of tensile strain on the conductivity depends on the purity (i.e., level of defects) of graphene. To clarify this, we have computed the conductivity of graphene with two hugely different levels of defect concentration.

Figure 12 shows the results for strained graphene with almost no defect (i.e., with $A_d = 9 \times 10^{-6}$). Our calculations reveal that the strain-related change in the conductivity is temperature dependent. In general, below room temperature we obtain both reduction as well as increase in the conductivity, depending on the amount of strain. Above room temperature the conductivity decreases for any magnitude of strain. In particular, our calculations reveal that the conductivity *decreases* with tensile strain for ϵ values of 0.003 and 0.006, but *increases* for ϵ values of 0.013 and 0.019. At 170 K, the conductivity decreases by 2.7% for $\epsilon = 0.006$ and increases

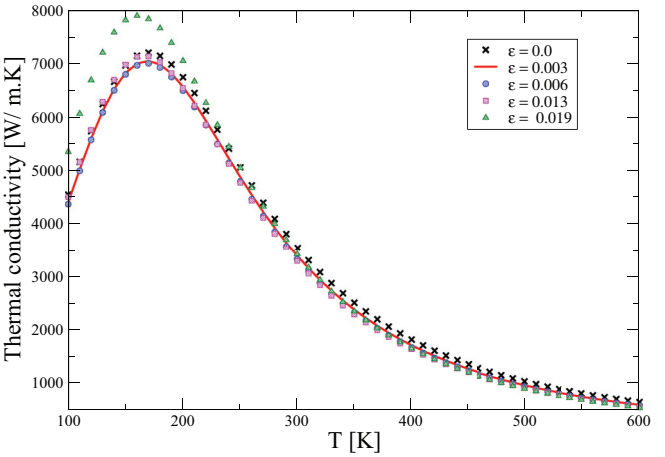

FIG. 12. (Color online) Thermal conductivity of defect-free graphene under tensile strain.

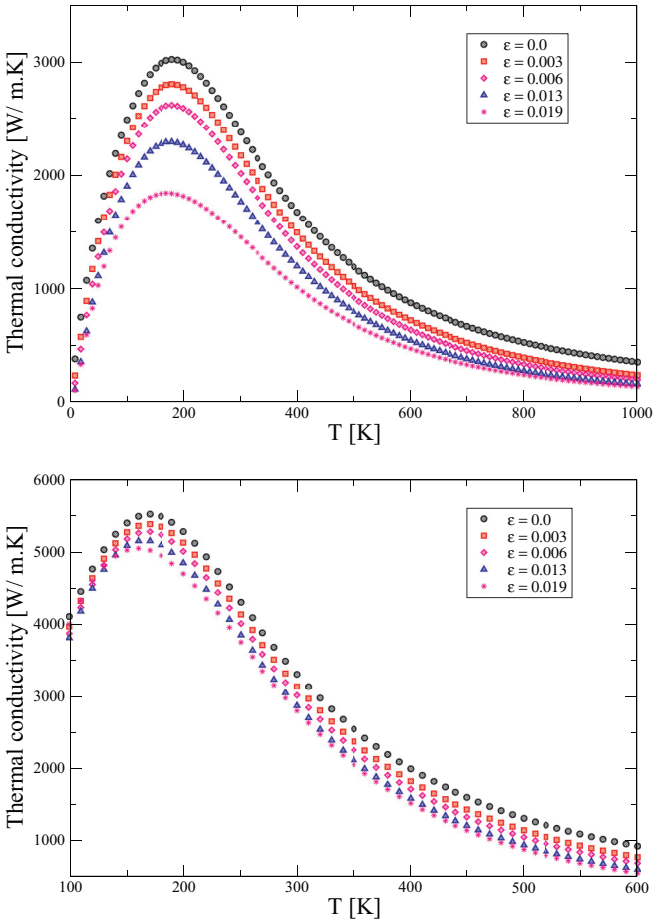

FIG. 13. (Color online) Effect of tensile strain on the thermal conductivity of graphene with different amounts of defects. The results shown in the lower and upper panels correspond to $A_d = 5.4 \times 10^{-5}$ and $A_d = 9 \times 10^{-4}$, respectively.

by 8.8% for $\epsilon = 0.019$. At 600 K, the conductivity decreases by 11% and 16% when ϵ is set at 0.006 and 0.019, respectively.

In the presence of finite amounts of defects, the effect of tensile strain is to reduce the thermal conductivity at all temperatures. This can be seen from the results presented in Fig. 13 for two defect concentrations: $A_d = 5.4 \times 10^{-5}$ and $A_d = 9 \times 10^{-4}$. The decrease in the conductivity for $A_d = 9 \times 10^{-4}$ and $\epsilon = 0.019$ is 39% at 170 K and 47% at 600 K. The decrease in the conductivity for $A_d = 5.4 \times 10^{-5}$ and $\epsilon = 0.019$ is 9% at 170 K and 41% at 600 K. These results clearly suggest that reduction in the conductivity becomes more pronounced for graphene with larger concentration of defects.

IV. SUMMARY

We have employed a semicontinuum theory for phonon dispersion relations, velocity, density of states, and Callaway's relaxation-time formalism in full to evaluate the thermal conductivity in graphene, in the graphite basal plane, and along the graphite c axis. The theory successfully explains the experimental measurements for these systems. For the considered samples, we find that throughout the temperature range, the conductivity of graphene is larger than that in the basal plane of graphite. In order to explain the huge reduction in the conductivity of graphite along its c axis we had to assume much stronger anharmonic interaction parameters, consistent with the fact that the in-plane Grüneisen parameter is smaller than that of the out-of-plane parameter. At low temperatures (up to 40 K), the thermal conductivity varies as $T^{1.6}$, $T^{2.4}$, and $T^{1.4}$ for graphene, in the graphite basal plane, and along the graphite c axis, respectively. Significant isotopic effect on the conductivity of graphene was found in the temperature range 50–300 K, with the maximum reduction at 200 K of 49% for 50% ^{13}C. The overall effect of strain is to increase the specific heat. It has been shown that the thermal conductivity of graphene can be significantly tuned with the combination of defect concentration and tensile strain. For pure graphene, in the presence of tensile strain the conductivity increases at low temperature, and decreases above room temperature. For graphene with point defects, the effect of strain is to reduce the conductivity at all temperatures. The decrease in the conductivity for the defect concentration $A_d = 9 \times 10^{-4}$ and strain parameter $\epsilon = 0.019$ is 39% at 170 K and 47% at 600 K.

ACKNOWLEDGMENT

A.A. gratefully acknowledges financial support from Taibah University, Madinah, Saudi Arabia.

*assa201@exeter.ac.uk; aalofi@taibah.edu.sa

[1] K. S. Novoselov, A. K. Geim, S. V. Morozov, D. Jiang, M. I. Katsnelson, I. V. Grigorieva, S. V. Dubonos, and A. A. Firsov, Nature (London) **438**, 197 (2005).

[2] Y. Zhang, Y. Tan, H. L. Stormer, and P. Kim, Nature (London) **438**, 201 (2005).

[3] D. L. Nika, E. P. Pokatilov, A. S. Askerov, and A. A. Balandin, Phys. Rev. B **79**, 155413 (2009).

[4] J. H. Seol, I. Jo, A. L. Moore, L. Lindsay, Z. H. Aitken, M. T. Pettes, X. Li, Z. Yao, R. Huang, D. Broido, N. Mingo, R. S. Ruoff, and L. Shi, Science **328**, 213 (2010).

[5] S. Ghosh, I. Calizo, D. Teweldebrhan, E. P. Pokatilov, D. L. Nika, A. A. Balandin, W. Bao, F. Miao, and C. N. Lau, Appl. Phys. Lett. **92**, 151911 (2008).

[6] G. A. Slack, Phys. Rev. **127**, 694 (1962).

[7] D. G. Onn, A. Witek, Y. Z. Qiu, T. R. Anthony, and W. F. Banholzer, Phys. Rev. Lett. **68**, 2806 (1992).

[8] E. Pop, V. Varshney, and A. K. Roy, MRS Bull. **37**, 1273 (2012).

[9] N. A. Abdullaev, Phys. Solid State **48**, 663 (2006).

[10] H. O. Pierson, *Handbook of Carbon, Graphite, Diamond and Fullerenes* (Noyes Publications, New Jersey, 1993).

[11]K. S. Novoselov, A. K. Geim, S. V. Morozov, D. Jiang, Y. Zhang, S. V. Dubonos, I. V. Grigorieva, and A. A. Firsov, Science **306**, 666 (2004).
[12]A. Yoshimori and Y. Kitano, J. Phys. Soc. Jpn. **11**, 352 (1956).
[13]B. T. Kelly and P. L. Walker, Carbon **8**, 211 (1970).
[14]B. T. Kelly, Carbon **12**, 535 (1974).
[15]L. A. Falkovsky, J. Exp. Theor. Phys. **105**, 397 (2007).
[16]N. Mounet and N. Marzari, Phys. Rev. B **71**, 205214 (2005).
[17]M. Mohr, J. Maultzsch, E. Dobardžić, S. Reich, I. Milošević, M. Damnjanović, A. Bosak, M. Krisch, and C. Thomsen, Phys. Rev. B **76**, 035439 (2007).
[18]B. T. Kelly, Carbon **6**, 71 (1968).
[19]B. T. Kelly, Carbon **5**, 247 (1967).
[20]J. Callaway, Phys. Rev. **113**, 1046 (1959).
[21]G. P. Srivastava, *The Physics of Phonons* (Adam Hilger, Bristol, 1990).
[22]G. P. Srivastava, J. Phys. Chem. Solids **41**, 357 (1980).
[23]T. Nihira and T. Iwata, Phys. Rev. B **68**, 134305 (2003).
[24]K. Komatsu and T. Nagamiya, J. Phys. Soc. Jpn. **6**, 438 (1951).
[25]P. G. Klemens and D. F. Pedraza, Carbon **32**, 735 (1994).
[26]G. A. Slack and S. Galginaitis, Phys. Rev. **133**, A253 (1964).
[27]C. A. Ratsifaritana and P. G. Klemens, Int. J. Thermophys. **8**, 737 (1987).
[28]S. Chen, Q. Wu, C. Mishra, J. Kang, H. Zhang, K. Cho, W. Cai, A. A. Balandin, and R. S. Ruoff, Nature (London) **11**, 203 (2012).
[29]V. Adamyan and V. Zavalniuk, J. Phys.: Condens. Matter **23**, 015402 (2011).
[30]M. D. Tiwari and B. K. Agrawal, Phys. Rev. B **4**, 3527 (1971).
[31]G. P. Srivastava, *High Thermal Conductivity Materials* (Springer Science/Business Media, New York, 2006), Chap. 1.
[32]J. M. Ziman, *Electrons and Phonons* (Clarendon, Oxford, 1960).
[33]C. Herring, Phys. Rev. **95**, 954 (1954).
[34]G. L. Guthrie, Phys. Rev. B **152**, 801 (1966).
[35]L. E. Fried and W. M. Howard, Phys. Rev. B **61**, 8734 (2000).
[36]R. G. Steg and P. G. Klemens, Phys. Rev. Lett. **24**, 381 (1970).
[37]D. L. Nika, S. Ghosh, E. P. Pokatilov, and A. A. Balandin, Appl. Phys. Lett. **94**, 203103 (2009).
[38]X. Li, K. Maute, M. L. Dunn, and R. Yang, Phys. Rev. B **81**, 245318 (2010).
[39]T. M. G. Mohiuddin, A. Lombardo, R. R. Nair, A. Bonetti, G. Savini, R. Jalil, N. Bonini, D. M. Basko, C. Galiotis, N. Marzari, K. S. Novoselov, A. K. Geim, and A. C. Ferrari, Phys. Rev. B **79**, 205433 (2009).
[40]Y. Wang, J. E. Panzik, B. Kiefer, and K. K. M. Lee, Sci. Rep. **2**, 520 (2012).
[41]P. L. de Andres, F. Guinea, and M. I. Katsnelson, Phys. Rev. B **86**, 144103 (2012).
[42]K. V. Zakharchenko, M. I. Katsnelson, and A. Fasolino, Phys. Rev. Lett. **102**, 046808 (2009).
[43]H. Zabel, J. Phys.: Condens. Matter **13**, 7679 (2001).
[44]F. Ma, H. B. Zheng, Y. J. Sun, D. Yang, K. W. Xu, and P. K. Chu, Appl. Phys. Lett. **101**, 111904 (2012).
[45]A. Alofi and G. P. Srivastava, J. Appl. Phys. **112**, 013517 (2012).
[46]S. Chen, A. L. Moore, W. Cai, J. W. Suk, J. An, C. Mishra, C. Amos. C. W. Magnuson, J. Kang, L. Shi, and R. S. Ruff, ACS Nano **5**, 321 (2011).
[47]A. DE Combarieu, J. Phys. **28**, 951 (1967).
[48]B. Dreyfus and R. Maynard, J. Phys. **28**, 955 (1967).
[49]D. T. Morelli and G. A. Slack, *High Thermal Conductivity Materials* (Ref. 31), Chap. 2.
[50]N. Wei, L. Xu, H. Wang, and J. Zheng, Nanotechnology **22**, 105705 (2011).
[51]D. L. Nika and A. A. Balandin, J. Phys.: Condens. Matter **24**, 233203 (2012).